On the cyclic bending behaviour of a hard coating on a ductile substrate with periodic surface hardened regions

Chen-Wu Wu *, Kun Zhang, Guang-Nan Chen

Institute of Mechanics, Chinese Academy of Sciences, No. 15 Beisihuanxi Road, Beijing 100190, China

ABSTRACT

A cyclic bending experiment is designed to investigate the interface fracture behaviour of a hard chromium coating on a ductile substrate with periodic surface hardened regions. The unique deflection pattern of the vertical cracks after they run through the coating and impinge at the interface is revealed experimentally. A simple double-layer elastic beam model is adopted to investigate the interfacial shear stresses analytically. A FE model is employed to compute the stresses of the tri-phase structure under a single round of bending, and to investigate the effect of the loading conditions on the deflection pattern of the vertical cracks at the interface.

© 2008 Elsevier Ltd. All rights reserved.

1. Introduction

The interface fracture shall arise between a hard coating and a ductile substrate under the action of the cyclic contacting and bending etc., which is largely due to the mismatch in stiffness of the coating and substrate (Hutchinson and Suo, 1992; Chai, 2003; Wu et al., 2006b). A great many of mosaic structures have been devised to release the mismatch, such as multilayer/grade coating (Bell et al., 1998; Matthews et al., 2001; Schwarzer, 2000; Chai and Ravichandran, 2007), and a hardened surface layer on the origin substrate by nitriding, carburizing or surface quenching, etc. (Fu et al., 2000; Podgornik and Vizintin, 2001).

Surface quenching has been adopted broadly to produce a hardened layer on the origin substrate (Bell et al., 1998). However, such a continuous hardened layer is indeed a secondary hard coating on the original substrate (Zhang et al., 2006), thereby introducing another interface between the hardened layer and the original substrate. Actually, the continuous surface hardened layer always faces the danger of buckling and spalling due to the relatively high compressive stress.

To overcome the above inadequacy, a novel complex coating has been devised by laser discrete quenching the steel substrate prior to plating the chromium coating as shown in Fig. 1(a) (Zhang et al., 2006; Wu et al., 2006a), in which the hardened regions are periodically obtained within the surface layer of the substrate. Therein, the chromium coating is approximately 250 μm, and the hardened region is repeated approximately every 5 mm. The HV numbers along a horizontal path through one period are plotted in Fig. 1(b) for three loci of different distances from the interface (dfi), which shows roughly the periodic fluctuation of the properties of the substrate. In fact, it is generally reported that such hardness increment in the as-quenched regions mainly due to the relatively high yielding stresses and residual compressive stresses therein (Li and Xiao, 1990; Qu and Wang, 1990). In particular, experiments show that the hardness number H is directly proportional to the material's yield stress Y, and can be expressed as $H = CY$. Herein C is called "constraint factor", and

---

* Corresponding author.
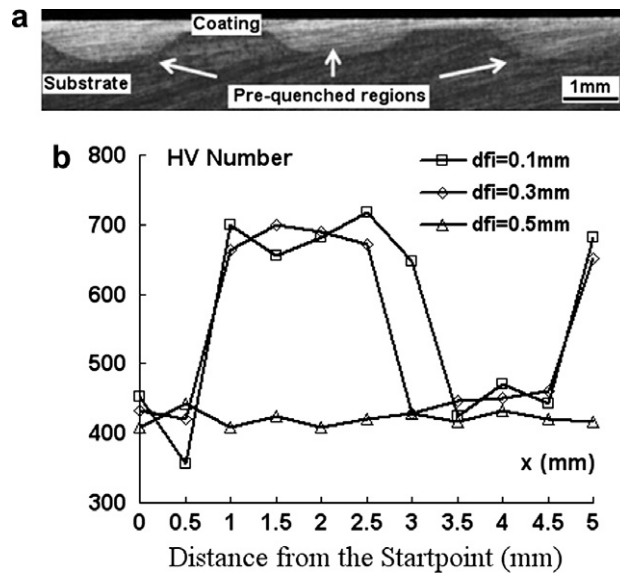 *E-mail address:* wcw_on@yahoo.com.cn (C.-W. Wu).

Fig. 1. (a) The profile of the specimen (Fu et al., 2000) and (b) HV number of the surface layer of the substrate as-quenched by CO_2 laser.

$C = 3$ for materials with a large value of the ratio E/Y (e.g., metal), where E is the elastic modulus (Cheng and Cheng, 1999; Anthony, 2002). Moreover, there are always residual tensile stresses in the intermediate regions between two adjacent as-quenched regions for a process of laser quenching without melting (Grevey et al., 1988; Rhima et al., 2003).

On such complex coatings, a series of investigations have been reported. Wu et al. (2006a) and Hu et al. (2005) reported that the thermal loading would introduce periodic segmentation cracks in the coating. These segmentation cracks are further reported by Wu et al. (2006b) and Wu et al. (2008) to be effective on decreasing the stress concentration around the interface corner when the spacing drop into certain range. Later on, Wu et al. (2007) revealed experimentally that the controllable cracking of the coating can also be developed when the specimen is subjected to in-plane tension, which is considered to be largely due to the unique pattern of the yielding stresses and residual stresses in the structure. Thereafter, Yang et al. (2007) investigated analytically the effect of the yielding stresses and residual stresses on the extension of the vertical crack into the as-quenched substrate by a meso-scale mechanical model, of which the prediction has been partly verified experimentally by this work.

In the present work, a cyclic bending experimental is design to investigate the fracture behaviour of this complex coating, with special attention being paid to the interface fracture. A simple analytic model and a FE model are utilised to describe the interfacial stresses and the deflections of the vertical cracks after they impinge at the interface.

2. Experiment and results

2.1. Description on the experiment

The specimens are produced under the procedure described as following. Firstly, the substrate, steel 30CrNi2MoVA is nonoverlapping quenched (the spacing between the centers of two adjacent tracks, i.e. the period is $W_p \approx 5$ mm) with CO_2 laser of power $P \approx 450$ W, beam diameter $D \approx 3$–4 mm and scanning velocity $v \approx 22.4$–28.2 mm/s. Then, a chromium coating of thickness 100 μm is plated on the substrate. Finally, specimens of required dimension are sliced and the cross sections are burnished for future observing and photographing. The cross section profile of the specimen is shown in Fig. 1(a) (Wu et al., 2006a). The HV numbers of the substrate close to the interface are plotted along a period as shown in Fig. 1(b), in which the gradient of the hardness is apparent.

A photo of the experimental apparatus and a sketch of the specimen are shown in Fig. 2(a) and (b), respectively. The total length of the specimen is about 50 mm. In Fig. 2(b), $R = 6$ mm representing the radii of the loading cylinder (above the specimen) and the two supporting cylinders (under the specimen), $t_s \approx 2$ mm is the thickness of the substrate, $t_c \approx 0.1$ mm is the thickness of the coating, $t_i \approx 1$ mm is the maximum thickness of the quenched region, $W_i \approx 4$ mm the maximum width of the quenched region and $W_p \approx 5$ mm the period. The dimension of the specimen perpendicular to the paper plane, b, is about 10 mm.

The cyclic loading steps are listed below in sequence, in which every round includes loading and unloading. To track the initiation of the damage as precisely as possible, the loading rounds are increased gradually with the loading steps.

Loading step b1: direct bending, during which the coating is compressed, for 1 round.
Loading step r1: reverse bending, during which the coating is tensioned, for 1 round.
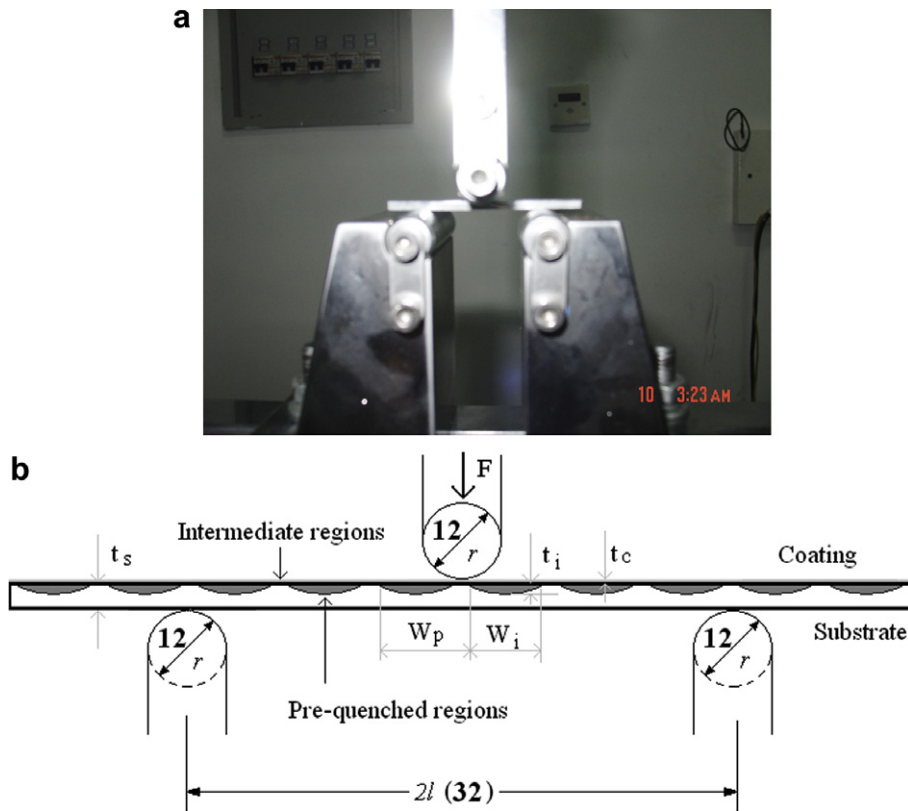
Fig. 2. (a) The loading equipment. (b) Sketch of the specimen.

Loading step b11: direct bending for 10 rounds.
Loading step r2: reverse bending for 1 round.
Loading step b111: direct bending for 100 rounds.
Loading step r3: reverse bending for 1 round.
Loading step b211: direct bending for 100 rounds.
Loading step r4: reverse bending for 1 round.

The experiment is carried out by controlling the displacement of the loading cylinder, with the maximum deflection of the specimen being approximately 1 mm for every round of every loading step. The rate of the deflection to time is chosen small enough to diminish the effect of the inertia. The total time for every round is approximately 30 s, of which about 20 s is for loading and 10 s for unloading.

2.2. Experimental results

The cyclic bending experiment was accomplished for 12 specimens of identical nominal dimensions. For every specimen, the cracking of the coating and the damage/fracture of the interface was tracked and photographed after every loading step. Finally the cross sections were etched with a solution of nitric acid with ethanol to display the locations of the cracks. Over 3000 photos were obtained, from which the typical cracking pattern have been extracted and the unique damage/fracture pattern has been revealed.

As an example, the interfacial shear stresses versus time during loading step b111 are depicted in Fig. 3. It is noted that the interfacial stress is derived from Eq. (6) (Section 3.1) using the recorded experimental data for the lateral forces. Such a simple derivation is based on the assumption of ideal elasticity and intact structure. In fact, the interfacial stresses should be very complicated if the effect of plasticity around the crack tip is taken into account. In Fig. 3, one can see that the peak value of the interfacial shear stresses decrease with increasing the load rounds. It is indicated that the bending stiffness of the specimen is reduced gradually. This may result from the extension of vertical and interface cracks. Moreover, as the vertical cracks in the coating are almost closed and retarded during direct bending, the reduction of the bending stiffness of the specimen should be largely due to the extending of the interface cracks.

It has been observed that the vertical cracks in the coating arose primarily during the slicing of the specimen and the loading step r1. In the former case, a tensile stress state is developed in the coating by the curvature of the specimen against the
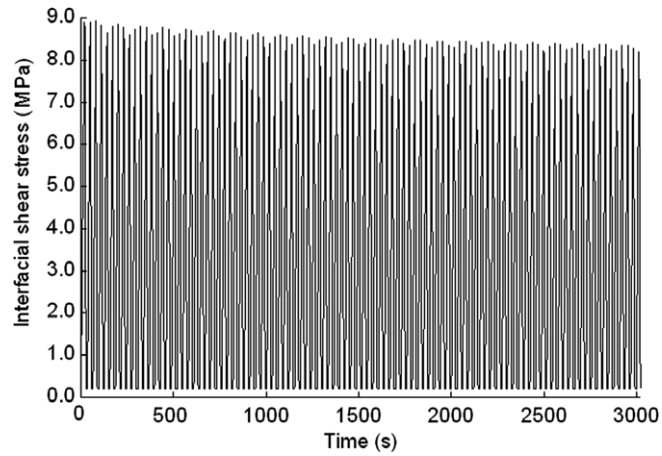
Fig. 3. Lateral force vs. time curve for bending (b111).

coating side, which is induced by the release of the residual compressive stress within the as-quenched layer of the substrate.

Several interface cracks arise between the coating and the as-quenched regions of the substrate for every specimen while no obvious interface fracture has been observed between the coating and the intermediate regions.
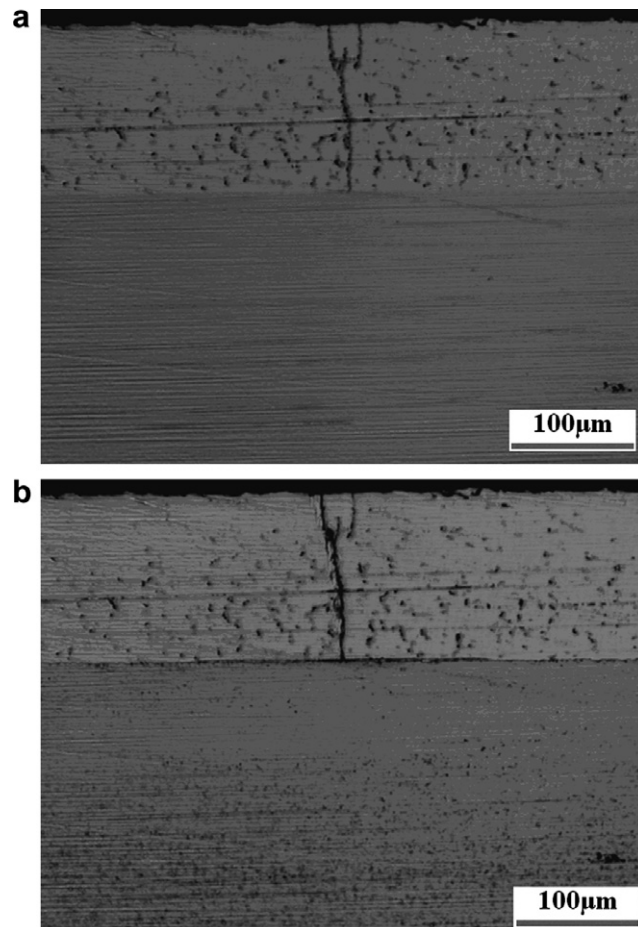

Fig. 4. (a) Coating/interface initial state. (b) Coating/interface after eroding.

Fig. 4(a) and (b) shows, respectively, the initial state and the final state of the region around a vertical crack in the coating, of which the latter is taken from the eroded specimen to show clearly the location of the crack. One can see that the interface crack is above the as-quenched region. To investigate the evolution of the vertical crack and the interface crack, the photos of the cross section have also been taken for several specified loading steps. To avoid the redundancy, only the photos of the initial state and final state are shown in Fig. 5a and b, respectively. By focusing on the photos after loading steps r1 and b11, which is not provided here for the sake of brevity, the interface crack can be observed around the initial vertical crack after loading steps r1 and b11. Moreover, it is found that, after the loading steps b211 and r4, the interface cracks extend slightly and even tend to be retarded. This means that the driving force for the interface fracture decreases with the extending of the interface cracks.

Fig. 6a and b displays the evolution of a vertical coating crack developed by the reverse bending and the evolution of the interface crack around it. Three vertical cracks arise in the coating after the first round of reverse bending, during which the coating is tensioned. An interface crack is observed right to the rightmost vertical crack after it impinges at the interface. However, left to this vertical crack or around the other two, there is no interface crack. This means that the interface stress is relatively low therein, which may be due to the effect of the vertical cracks on relaxing the stresses (Wu et al., 2008).

Fig. 7(a) and (b) demonstrates the extending of another initial vertical crack above the as-quenched region. This vertical crack impinges at the interface and penetrates into the substrate without initiating any obvious interface crack. This may be again due to the existence of the other vertical cracks around, which is considered to be able to relax the interface stresses as discussed in the aforementioned case.

Fig. 8(a) and (b) demonstrates the evolution of a vertical crack in a coating bonded to the intermediate region of the substrate, which represents the extending character of almost all of the vertical cracks above the intermediate regions. The vertical crack penetrates straightly into the substrate, and induces strain localization within the substrate. There is no obvious interface crack around them.

As demonstrated herein, the experimental results reveal that a few interface cracks arise around certain vertical cracks in a coating bonded to the as-quenched regions, whereas no interface cracks are observed around the vertical cracks in a coating bonded to the intermediate regions. This is because the residual compressive stresses within the substrate always retard the penetration of the vertical coating crack into it, while the residual tensile stresses induce such penetration. Thus, the theoretical prediction by Yang et al. (2007) is partly verified, in which it is reported that the as-quenched layer shall retard the
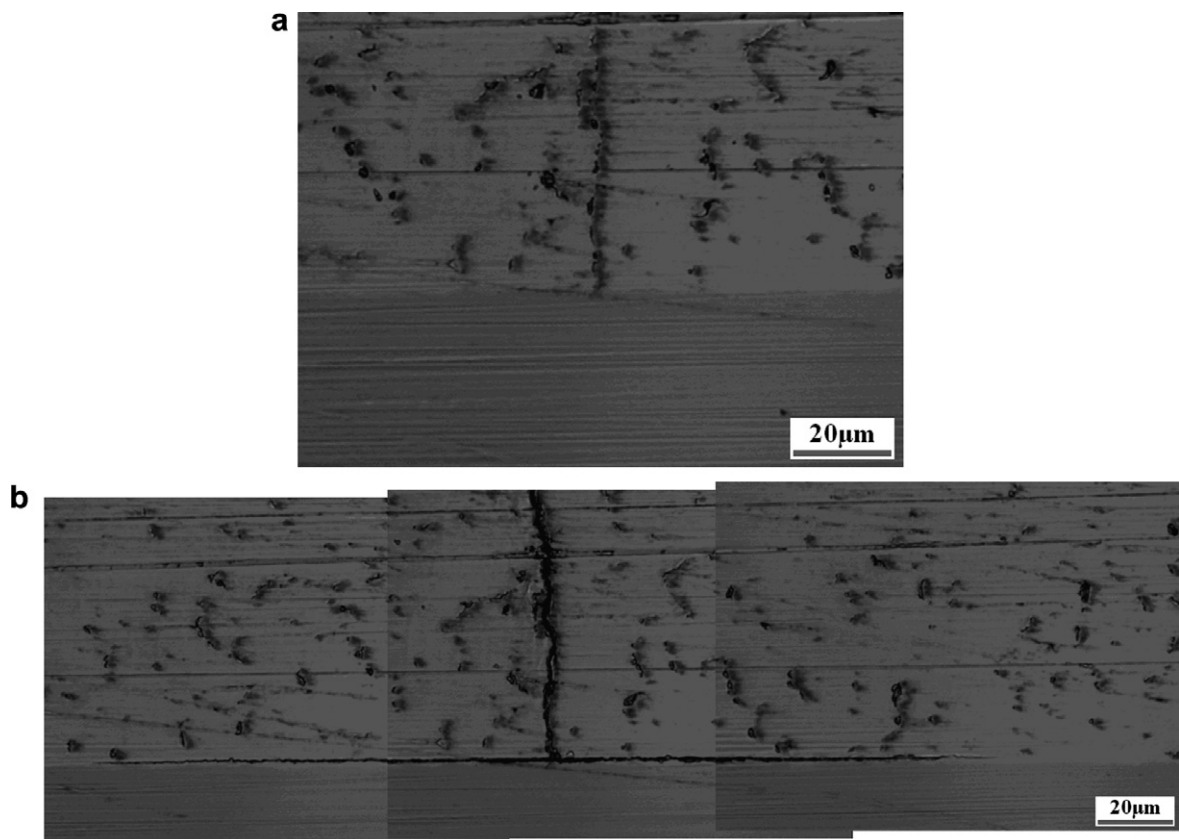

Fig. 5. (a) Coating/interface in initial state. (b) Coating/interface after r4.
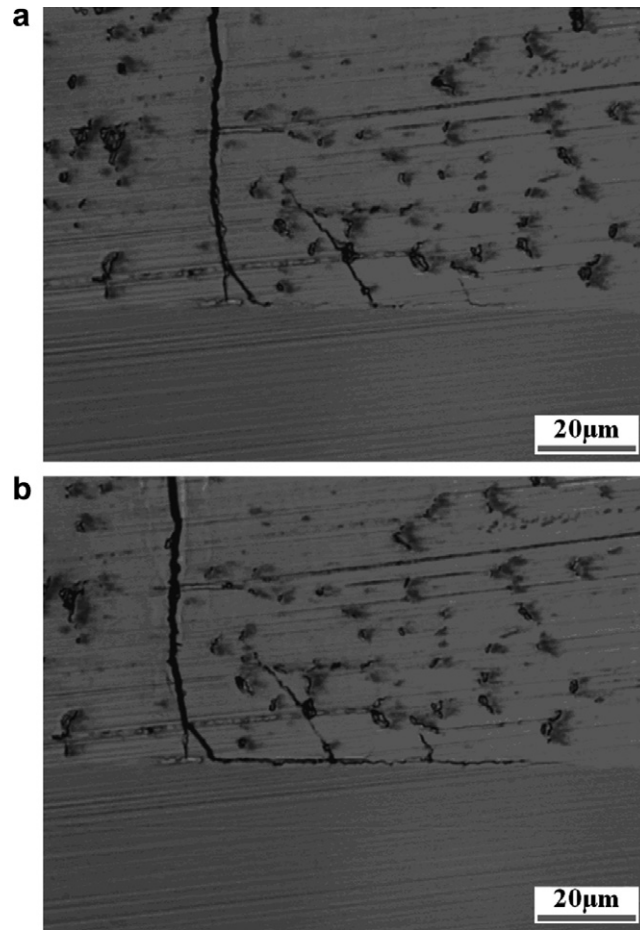
Fig. 6. (a) Coating/interface after r1. (b) Coating/interface after r4.

penetrating of a vertical crack into the substrate. These results also indicate that a continuous surface quenched layer may induce severe interface fractures when the specimen is subjected to cyclic bending. But the periodic distributed intermediate regions between two adjacent as-quenched regions may partition, even hold back the interface crack. It is indicated that such periodic subsurface structure have some superiority in preventing the enormous linking up of the interface cracks, which is considered to be critical for the debonding of the coating.

3. Mechanical analysis and numerical calculation

To demonstrate the stress state of the specimen under bending, preliminary analytical modeling is presented firstly. However, considering the complexity of the geometry of the specimen and the nonlinear behaviours of the materials, the analytical model is deemed qualitative. To investigate the deflection of the vertical cracks, finite element modeling is further adopted. Moreover, as the dimension of the plastic regime around the crack tip is similar to the crack length and unloading is involved in the experimental, the present available fracture parameters such as stress intensity factor and J integral can not be applied directly (Meguid, 1989; Kanninen and Popelar, 1985). Thus, the mechanical behaviour of the cracked body shall be roughly characterized with energy method herein.

3.1. Mechanical analysis

For simplicity, the effect of the cracking and the plasticity are not involved in the analytical modeling, which indicates that the model of double-layer elastic beam is applicable. The cell of the specimen consists of the substrate and coating is depicted in Fig. 9. The elastic moduli of the substrate and the coating are E_s and E_c, respectively.

Rectangular coordinates are used as shown in Fig. 9, with Z-axis at the intersection line of the neutral plane and the symmetry plane of the cell, and X-axis perpendicular to the neutral plane. The thickness of the coating is $t_c = 0.1$ mm, the thick-
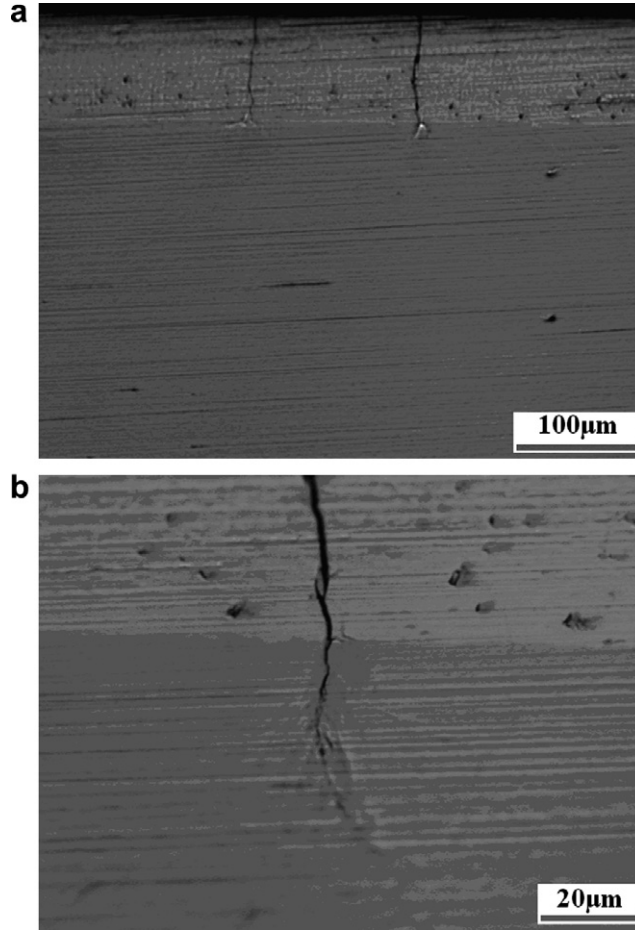
Fig. 7. (a) Coating/interface after r1. (b) Coating/interface after r4.

ness of the substrate is $t_s = 2$ mm, the maximum thickness of the as-quenched region is $t_i = 1$ mm, and the dimension perpendicular to the paper plane XOY is $b = 10$ mm. With denoting the location of the bending center by h_{bc}, one obtains

$$h_{bc} = \frac{E_s t_s^2 + E_c t_c^2 + 2E_c t_c t_s}{E_s t_s + E_c t_c}$$

With reference to the bending theory of the elastic composite beam (Timoshenko and Goodier, 2004), the stresses can be obtained instantly.

The effective bending stiffness

$$\langle EI \rangle = E_c \left(\frac{bt_c^3}{12} + \left(\frac{t_c}{2} + t_s - h_{bc} \right)^2 bt_c \right) + E_S \left(\frac{bt_s^3}{12} + \left(\frac{t_s}{2} - h_{bc} \right)^2 bt_s \right)$$

The normal stress of the coating

$$\sigma_{yyc} = \frac{M_z E_c}{\langle EI \rangle} x \tag{1}$$

The normal stress of the substrate

$$\sigma_{yys} = \frac{M_z E_s}{\langle EI \rangle} y \tag{2}$$

The shear stress of the coating

$$\tau_{xyc} = \frac{Q}{\langle EI \rangle} \frac{E_c((t_c + t_s - h_{bc})^2 - x^2)}{2} \tag{3}$$
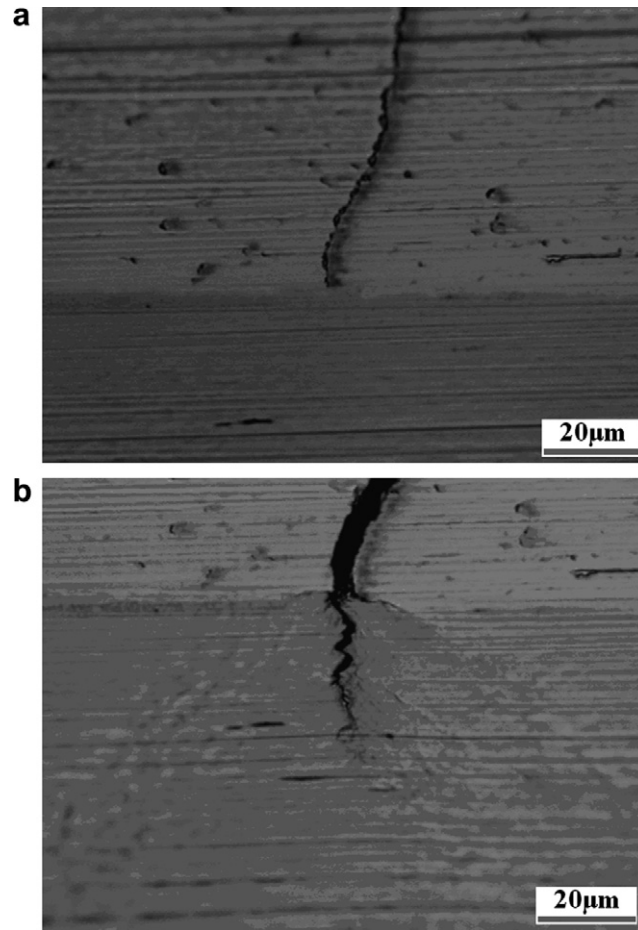
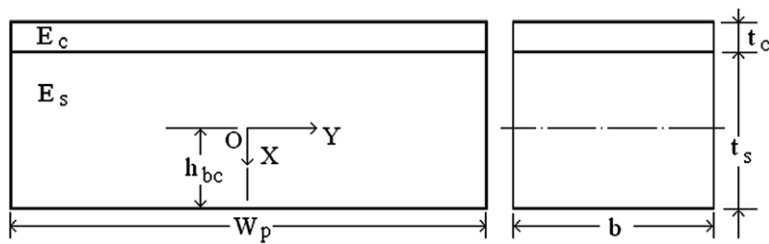Fig. 8. (a) Coating/interface in initial state. (b) Coating/interface after r4.

Fig. 9. Sketch of the cell under bending.

The shear stress of the substrate

$$\tau_{xys} = \frac{Q}{\langle EI \rangle} \frac{E_c((t_c + t_s - h_{bc})^2 - (t_s - h_{bc})^2) + E_s((t_s - h_{bc})^2 - x^2)}{2}, \quad x \leqslant 0 \tag{4}$$

$$\tau_{xys} = \frac{Q}{\langle EI \rangle} \frac{E_s(h_{bc}^2 - x^2)}{2}, \quad x > 0 \tag{5}$$

In the above formula, the bending moment $M_z = F(l - \bar{y})/2$, herein F is the loading force as shown in 2, $\bar{y}$ is the horizontal distance from the center of the loading cylinder. And $Q = F/2$ right to the loading cylinder, $Q = -F/2$ left to the loading cylinder.

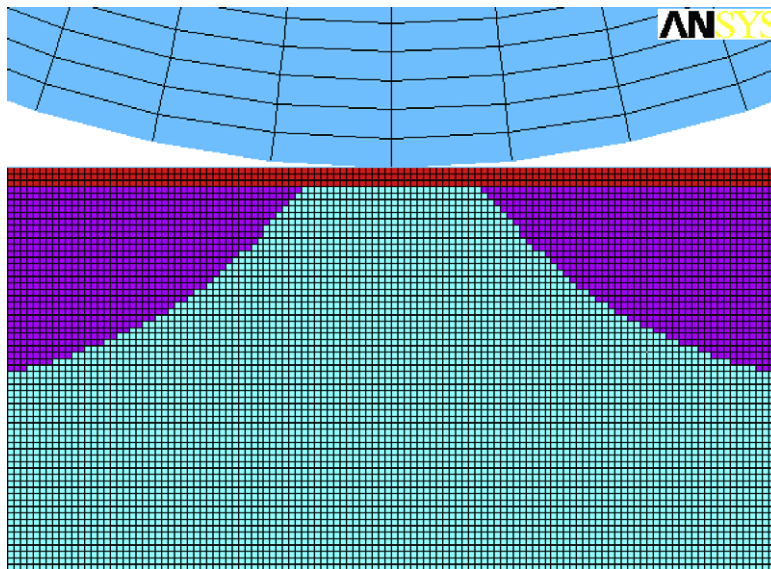Further, one can obtain the interfacial shear stress

Fig. 10. Sketch of the part of the elements (responding to the case of direct bending).

$$\tau_i = \frac{Q}{\langle EI \rangle} \frac{E_c((t_c + t_s - h_{bc})^2 - (t_s - h_{bc})^2)}{2} \tag{6}$$

This simple analysis is applicable only to the structure of ideal elastic materials without cracking. The post-yielding and post-cracking behaviour of the specimen is simulated by the FEM focusing on the crack deflection around the interface.

3.2. Numerical model

The FE model, consisting of coating, substrate and as-quenched regions, is shown in Figs. 2(b) and 10. In the computations the contact boundaries are adopted between the supporting/loading cylinders and the specimen. Firstly, the stress fields are obtained for the intact specimen under direct bending and reverse bending, respectively. Then, the deflection of the vertical crack is discussed after it runs through the coating.

As depicted in Fig. 2(b), a relative sliding is allowed between the supporting/loading cylinders and the specimen. The coating and substrate are assumed perfectly bonded, except for the case when the interface crack is taken into account. Thus, two kinds of models on the interfaces shall be adopted in the analysis:

One is the sliding interface for the contacting status between the supporting/loading cylinders and the specimen, as well as between the crack faces. The boundary conditions for such interfaces can be written as $\sigma_n^+ = \sigma_n^-$, $\sigma_\tau^+ = -\sigma_\tau^- = k\sigma_n$ and $u_n^+ = u_n^-$. Herein σ represents the tractions intensity acted at the interface with the subscript n and τ denoting the directions of normal and tangent, respectively. k is the coefficient of friction. The symbol u is the displacement with '+' and '−' correspond to the materials points of the two sides at the interface.

The other is the perfect bonded interface for the joined status between the coating and the substrate. The boundary conditions for such interfaces can be written as $\sigma_n^+ = \sigma_n^-$, $\sigma_\tau^+ = -\sigma_\tau^-$, $u_n^+ = u_n^-$ and $u_\tau^+ = u_\tau^-$ (Erdogan, 1997).

As shown in Fig. 2(b), the vertical displacements of the horizontal axial plane of the two supporting cylinders are completely constrained, and that of the loading cylinder is specified by values dependent on the load stages. The mechanical behaviours of the coating and the loading/ supporting cylinders are assumed to be ideally elastic and the substrate elastic perfectly plastic. The yielding stresses of the original substrate and the as-quenched regions are σ_{yo} and σ_{yh}, respectively. The mechanical properties used in the simulation are listed in Table 1 (Zhang, 1989; Safranek, 1974), in which the cylinders represent the loading/supporting cylinders.

Table 1
Mechanical properties of the materials (Zhang, 1989; Safranek, 1974)

	Elastic modulus (MPa)	Poisson's ratio	Yielding stress (MPa)
Coating (chromium)	260e9	0.2	–
Origin substrate	202e9	0.255	800
Quenched substrate	202e9	0.255	800×1.5
Cylinders	200e9	0.3	–

3.3. Numerical results

In Fig. 11(a) and (b), the average stresses in Y direction, $\overline{\sigma_{yy}} = \frac{1}{t_c}\int_0^{t_c}\sigma_{yy}\,dy$, are depicted for the cases of direct bending and reverse bending, respectively. The results shown in Fig. 11(a) indicate that there are only compressive stresses within the coating under loading and unloading for the case of direct bending. The results shown in Fig. 11(b) indicate that only tensile stresses arise within most of the coating for the case of reverse bending, and the small compressive stresses appearing within the regions contacted by the supporting cylinder disappear completely after unloading. Thus, it is natural to conclude that the coating cracking should have been developed during the reverse bending, because only the tensile stresses in the coating can lead to cracking.

In Figs. 12 and 13, the interfacial stresses are depicted for both cases of direct bending and reverse bending, respectively. Considering the fact that the interfacial stresses are highly concentrated round the symmetry plane of the specimen, only the range of 1.5 Wp right to the loading cylinder is focused on for a clear description. It is shown that the interfacial normal stresses are mainly compressive for the case of direct bending (shown in Fig. 12(a)) and tensile for reverse bending (shown in
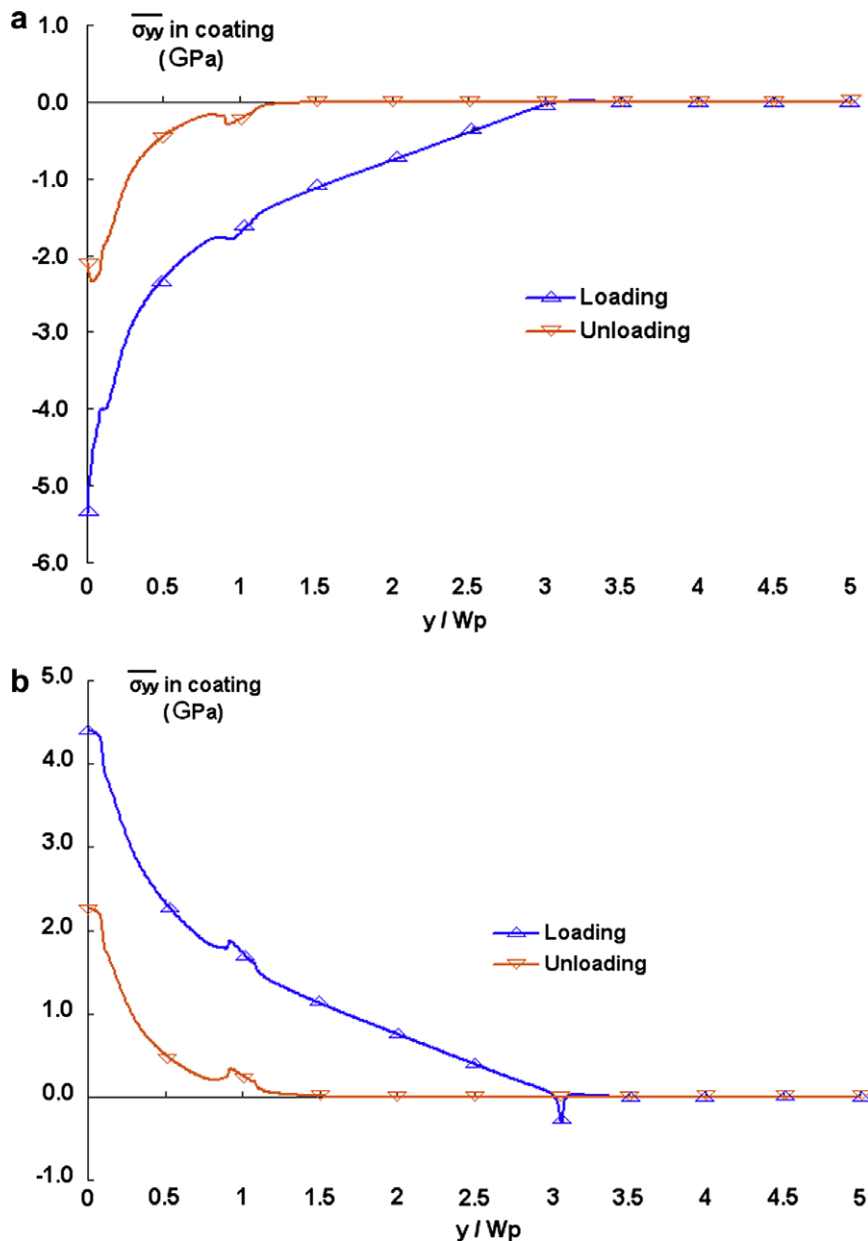

Fig. 11. (a) Tensile stress σ_{yy} in coating for direct bending. (b) Tensile stress σ_{yy} in coating for reverse bending.
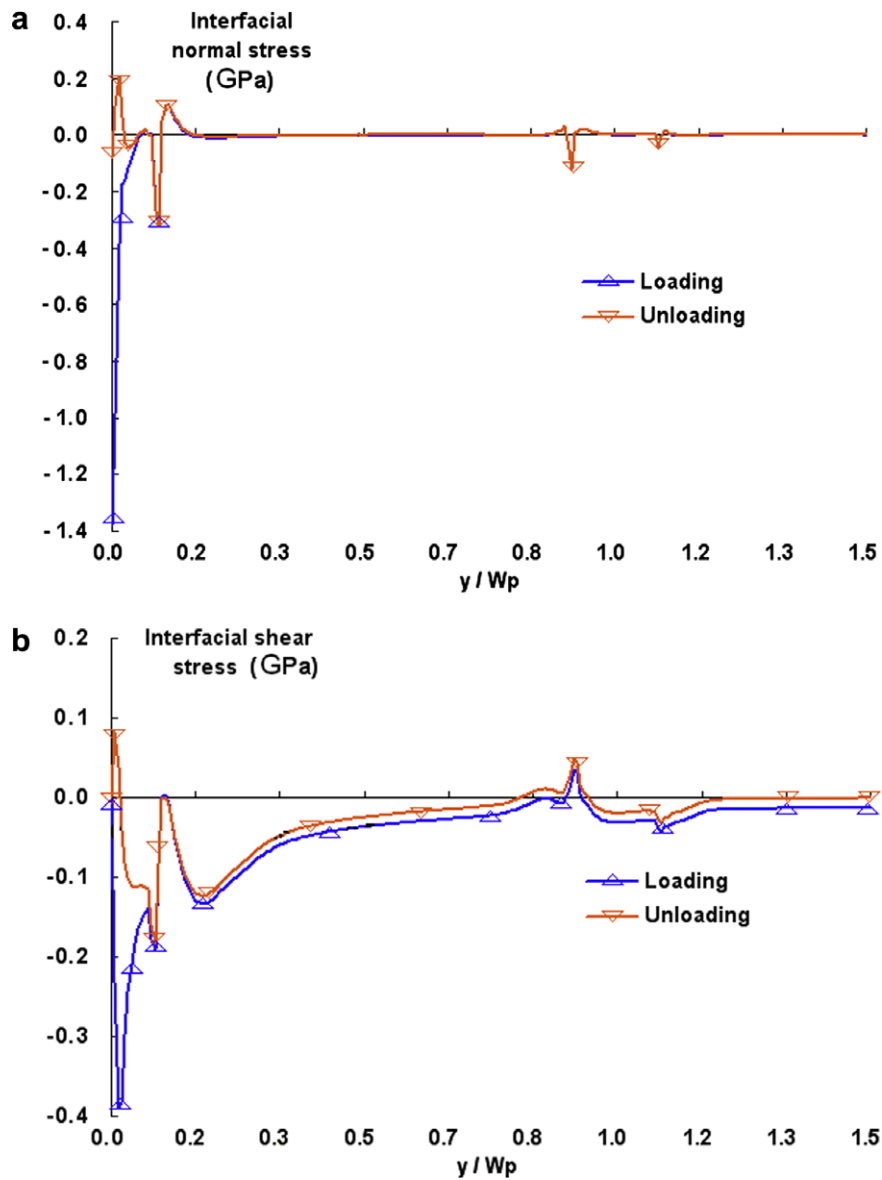
Fig. 12. (a) Interfacial normal for direct bending. (b) Interfacial shear stress for direct bending.

Fig. 13(a)), both of which are too localized to be of effect on the interface fracture. However, the interfacial shear stresses arise within the relatively large regime of the interface as shown in Figs. 12(b) and 13(b). And the direction of the shear stress in direct bending is opposed to that in reverse bending, which thus produces a cyclic altering shear stress state in the interface. These results indicate that the interface fracture is more likely to be induced by the cyclically altering interfacial shear stresses. This is in consistent with that predicted by the analytic analysis as aforementioned.

Figs. 12(b) and 13(b) show the interfacial shear stresses in the case of direct bending, which are apparently greater than that of reverse bending. This indicates that interfacial fracture is largely due to the direct bending. To justify this assumption, the tri-phase structure with a vertical crack above the center of the as-quenched region is modeled as shown in Fig. 14(a). The method of virtual crack extension (Parks, 1977) is adopted to compare the average energy release rate for the two situations, that is, the vertical crack extends straightly into the substrate by length αt_c (as shown in Fig. 14(b)) and deflects into the interface by length αt_c (as shown in Fig. 14(c)). Herein, the factor $\alpha = 1$ is adopted, by which results with acceptable accuracy are achieved. First, the elastic strain energy W_e and the plastic work W_p of the specimen are calculated for the three states, i.e. the vertical crack impinges at the interface (denoted by the superscript Cc), the vertical crack extends straightly into the substrate (denoted by the superscript Sc) and the vertical crack deflect into the interface (denoted by the superscript Ic). Then a dimensionless parameter of relative energy release rate can be defined as
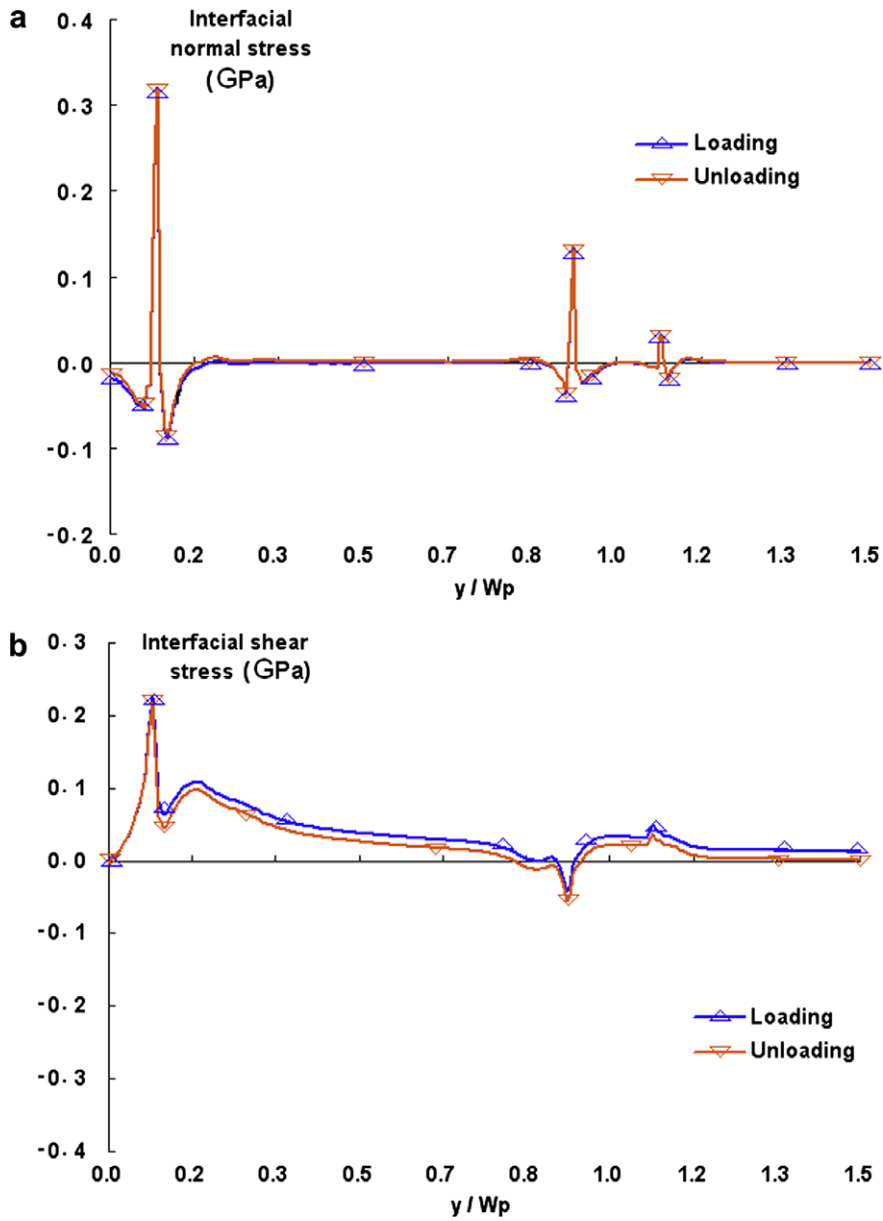
Fig. 13. (a) Interfacial normal stress for reverse bending. (b) Interfacial shear stress for reverse bending.
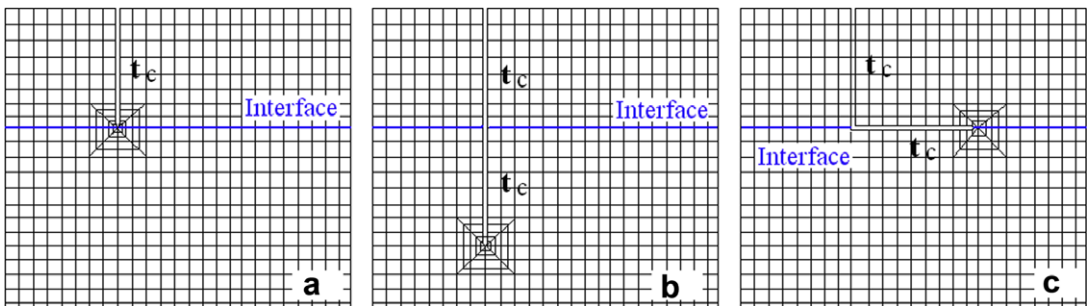

Fig. 14. Sketch of the crack (a) in coating (b) penetrating into substrate (c) deflecting into interface.
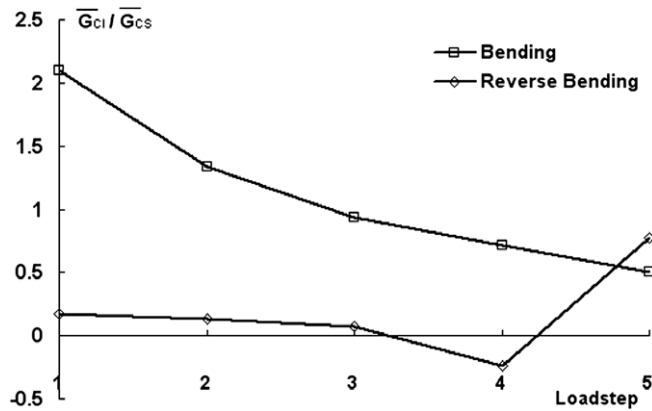
Fig. 15. $\overline{G_{CI}}/\overline{G_{cs}}$ for direct bending and reverse bending.

$$\frac{\overline{G_{CI}}}{\overline{G_{CS}}} = \frac{(W_e^{Cc} - W_e^{Ic}) - (W_p^{Ic} - W_p^{Cc})}{(W_e^{Cc} - W_e^{Sc}) - (W_p^{Sc} - W_p^{Cc})}$$

Following He and Hutchinson (1989), it is reasonable to assume that if $\frac{\overline{G_{CI}}}{\overline{G_{cs}}} \leqslant \frac{\Gamma^I}{\Gamma^s}$, the vertical crack extends into the substrate. If $\frac{\overline{G_{CI}}}{\overline{G_{cs}}} > \frac{\Gamma^I}{\Gamma^s}$, the crack would deflect into the interface. Here the parameters Γ^I and Γ^s represent the fracture toughness of the interface and the substrate, respectively. Of course, it is generally accepted that the toughness of the interface, Γ^I, is dependent on the mix mode of the loading on the interface. However, only the dimensionless parameter $\frac{\overline{G_{CI}}}{\overline{G_{cs}}}$ is of interest herein, on which the effects of loading situations, i.e. direct bending or reverse bending, and the loading stages shall be discussed. The values of $\frac{\overline{G_{CI}}}{\overline{G_{cs}}}$ against the loading stages are plotted in Fig. 15, where points No. 1, No. 2, No. 3 and No. 4 correspond to the relevant loading level, and point No. 5 the unloading status.

It is apparent from Fig. 15 that during loading, the values of $\frac{\overline{G_{CI}}}{\overline{G_{cs}}}$ for the case of direct bending are always greater than that of reverse bending. This means that the interface damages are developed more likely in direct bending. However, when unloading, the value of $\frac{\overline{G_{CI}}}{\overline{G_{cs}}}$ for the case of reverse bending is greater than that of the direct bending. This indicates that, during unloading the reverse bending may contribute more to the interface damages.

Finally, it is to be noted that only a single round of bending, either direct bending or reverse bending is simulated herein. Therefore, no calculations of plastic deformation are involved, which may influence the stress field and the interface fracture. We should also take note that the residual stresses distributed periodically within the surface layer of the substrate have not been included in this calculation. In fact, such a residual stress state would lead to great increase in the resistance of the vertical crack extending into the as-quenched regions and increasing the driving force extending into the origin substrate. This has also been argued by Yang et al. (2007). Thus, in effect, above the as-quenched regions, the driving force for the vertical crack deflecting into the interface shall be strengthened.

4. Conclusions

Cyclic bending has been conducted on the hard coating on a substrate with periodic surface as-quenched regions. The experimental results show that the interface cracks arise only above the as-quenched regions. Every vertical crack in the coating on the intermediate regions between two adjacent as-quenched regions penetrates straightly into the substrate. It is indicated that such a periodic subsurface structure have some superiority in preventing the enormous linking up of the interface cracks, which is considered to be critical for the debonding of the coating.

Stress results from a simple analytic model and the FE model reveal that the interfacial shear stresses should contribute mainly to the interface fracture. The interfacial shear stresses during loading for the case of direct bending are greater than that of reverse bending, although this difference is reduced apparently after unloading. This indicates that the interface fracture may be mainly due to the direct bending.

A relative energy release rate, $\overline{G_{CI}}/\overline{G_{cs}}$, has been brought forward and computed by a FE model to investigate the effects of the loading stages and loading situations. During loading, the parameter $\overline{G_{CI}}/\overline{G_{cs}}$ for the case of direct bending is greater than that of reverse bending, which indicates again the interface damages may be induced mainly by the direct bending. However, after unloading, $\overline{G_{CI}}/\overline{G_{cs}}$ for the case of direct bending is less than that of reverse bending, which shows that the unloading, especially for the case of reverse bending may also be partly the cause of the interface fracture.

Acknowledgements

References

Anthony, C.F., 2002. Nanoindentation. Springer, New York.

Bell, T., Dong, H., Sun, Y., 1998. Realising the potential of duplex surface engineering. Tribology International 31, 127–137.

Chai, H., 2003. Fracture mechanics analysis of thin coatings under plane-strain indentation. International Journal of Solids and Structures 40, 591–610.

Chai, H., Ravichandran, G., 2007. Transverse fracture in multilayers from tension and line-wedge indentation. International Journal of Fracture 145, 299–312.

Cheng, Y.T., Cheng, C.M., 1999. Scaling relationships in conical indentation of elastic perfectly plastic solids. International Journal of Solids and Structures 36, 1231–1243.

Erdogan, F., 1997. Fracture mechanics of interfaces. In: Rossmanith, H.-P. (Ed.), Damage and Failure of Interfaces. A.A. Balkema Publishers, Brookfield.

Fu, Y.Q., Wei, J., Yan, B.B., Loh, N.L., 2000. Characterization and tribological evaluation of duplex treatment by depositing carbon nitride films on plasma nitrided Ti-6Al-4V. Journal of Materials Science 35, 2215–2227.

Grevey, D., Maiffredy, L., Vannes, A.B., 1988. A simple way to estimate the level of the residual stresses after laser heating. Journal of Mechanical Working Technology 16 (1), 65–78.

He, M.-Y., Hutchinson, J.W., 1989. Kinking of a crack out of an interface. Journal of Applied Mechanics 56, 270–278.

Hu, Y., Zhang, K., Chen, G.N., Wu, C.W., 2005. MATLAB used in analyzing the microcracks of Cr coating. Heat Treatment of Metal 30 (Suppl.), 161–164 (in Chinese).

Hutchinson, J.W., Suo, Z., 1992. Mixed-mode cracking in layered materials. Advances in Applied Mechanics 29, 63–191.

Kanninen, M.F., Popelar, C.H., 1985. Advanced Fracture Mechanics. Oxford University Press, New York.

Li, H.-D., Xiao, J.M. (Eds.), 1990. Surfaces and Interfaces of Materials. Tsinghua University Press, Beijing (in Chinese).

Matthews, A., Jone, R., Dowey, S., 2001. Modelling the deformation behaviour of multilayer coatings. Tribology Letters 11, 103–106.

Meguid, S.A., 1989. Engineering Fracture Mechanics. Elsevier Applied Science, London and New York.

Parks, D.M., 1977. The virtual crack extension method for nonlinear material behaviour. Computer Methods in Applied Mechanics and Engineering 12, 353–364.

Podgornik, B., Vizintin, J., 2001. Influence of substrate treatment on the tribological properties of DLC coatings. Diamond and Related Materials 10, 2232–2237.

Qu, J.X., Wang, H.-H. (Eds.), 1990. Handbook for Surface Engineering. Chemical Industry Press, Beijing (in Chinese).

Rhima, A.B., Bessrour, J., Bouhafs, M., Khadrani, R., 2003. An idealisation of the residual stresses genesis in heat treatments by a laser moving source. International Journal of Thermal Sciences 42, 759–776.

Safranek, W.H. (Ed.), 1974. The Properties of Electrodeposited Metals and Alloys: A Handbook. Elsevier, New York.

Schwarzer, N., 2000. Coating design due to analytical modelling of mechanical contact problems on multilayer systems. Surface and Coatings Technology, 397–402.

Timoshenko, S.P., Goodier, J.N., 2004. Theory of Elasticity, third ed. Tsinghua University Press, Beijing.

Wu, C.-W., Chen, G.-N., Zhang, K., Hu, Y., Liang, N.-G., 2006a. On the formation of periodic segmentation cracks in a coating plated on a substrate with periodic subsurface inclusions. Surface and Coatings Technology 201, 2364–2368.

Wu, C.-W., Chen, G.-N., Zhang, K., Luo, G.-X., Liang, N.-G., 2006b. The effect of periodic segmentation cracks on the interfacial debonding: study on interfacial stresses. Surface & Coatings Technology 201, 287–291.

Wu, C.-W., Chen, G.-N., Zhang, K., Liang, N.-G., 2008. On the interaction of channeling/segmentation cracks of coating: Study on the critical spacing. Engineering Fracture Mechanics 75, 2531–2541.

Wu, C.-W., Yang, B.-Q., Chen, G.-N., Zhang, K., Xiao, J.-H., 2007. On the tensile behaviours of a hard chromium coating plated on a steel substrate with periodic subsurface inclusions. Surface & Coatings Technology 201, 7699–7705.

Yang, B.-Q., Zhang, K., Chen, G.-N., Luo, G.-X., Xiao, J.-H., 2007. Effect of a laser as-quenched steel substrate surface on the crack driving force in a coating-steel substrate system. Acta Materialia 55 (13), 4349–4358.

Zhang, K., Wu, C.-W., Hu, Y., Chen, G.-N., 2006. The design and application of a novel duplex coating formed by laser pre-treatment. Solid State Phenomena 118, 243–246.

Zhang, Z.X. (Ed.), 1989. Handbook of Enginery Metal materials. Weapon Industry Press, Beijing (in Chinese).